

Mechanical Properties of Glulam Moment-Resisting Joints Reinforced by Inclined Self-Tapping Screws

Shuo Wang,^a Panpan Ma,^a Jingkang Lin,^b Tongyu Hou,^a Feibin Wang,^a Zeli Que,^{a,*} and Meng Gong^c

Self-tapping screws (STS) are an effective fastener to enhance wooden moment-resisting joints. However, the effects of the arrangement and insertion angle of STS on the mechanical properties of wooden joints are less studied. Therefore, this study investigated the influence of these two factors on the mechanical properties of wooden joints by conducting cyclic loading tests using glulam moment-resisting joints reinforced by STS with different arrangements (round and square) and insertion angles (45° and 90°). The failure modes, bearing performances, and energy dissipation capacities were considered. The results showed that the insertion angle affected the bearing and energy dissipation capacity of the joints significantly, while the effect of arrangement was slight. The anti-rotation bending moments of the joints reinforced by inclined STS were higher by 31.7% and 13.5% when the arrangement of STS was circular and rectangular respectively compared with the joints reinforced by vertical STS under compression state, and were lower by 17.5 % and 22.9 % under tensile state. The restoring force characteristics of the joints were similar when the insertion angle of STS was the same. Furthermore, the joints had optimal ductility and stiffness when the arrangement was rectangular, and the insertion angle was 45°.

DOI: 10.15376/biores.19.2.2626-2638

Keywords: Moment-resisting joint; Self-tapping screw; Inclined driving angle; Glulam; Cyclic loading

Contact information: a: Nanjing Forestry University, Nanjing, Jiangsu, 210037, China; b: Fujian Provincial Institute of Architectural Design and Research Co., Ltd, Fuzhou, Fujian, 350001, China; c: Wood Science and Technology Centre, University of New Brunswick, Fredericton, NB, Canada; * Corresponding author: zeliq@njfu.edu.cn

INTRODUCTION

In a beam-column timber system, the moments can be transferred only by moment-resisting joints. At present, beam-column joints in timber structures generally adopt built-in steel plates and are connected by bolts (Lam *et al.* 2008). Although making connections by steel plates and bolts is an effective method to enhance the bearing capacity of moment-resisting joints, this method has an unavoidable disadvantage of inefficient fabrication processing because the wood must be slotted and drilled in advance. In addition, the cross-section of the wooden joints may be damaged due to slotting and drilling, which will then weaken the joints to a certain extent (Jensen 2005).

To replace the use of steel plates and bolts in the connection of beam-column joints, various measures have been proposed by scholars recently. These include the use of tooth plates (Hans *et al.* 2011), fiber composites like carbon fiber-reinforced polymers (Kasal *et al.* 2004), and self-tapping screws (STS) (Mirdad *et al.* 2022). Among different methods, STS have the advantage of simplicity, efficiency, and cost-effectiveness because they do

not require pre-drilling the timber, and the cross-section of the wood will then not be damaged (Lam *et al.* 2010). Accordingly, STS have been recognized as one of the most advanced fasteners for timber structures.

STS were used as tensile or compressive reinforcements in dowel and other types of joints to transfer the tensile forces perpendicular to the grain (Bejtka and Bl 2004). Researchers found that during the stress process, the tensile stress and the shear stress generated within a self-tapping screw could be transmitted through the bonding of the wood fibers wound around the screw and were contributed to the delay of wood cracking, thereby changing the failure mode of the joint from brittleness to ductility and improving the load capacity and ductility of the joint effectively (Gehloff *et al.* 2010). For optimization of the load capacity of the wooden joint reinforced by STS, the effect of the STS configuration on mechanical properties of wooden joint were studied. The results showed that in addition to the influence of the type of STS, the diameter of the STS and embedment depth, the insertion angle and the arrangement of STS also affected the bearing performance of the base pin groove, the nail-holding force, and the lateral shear performance significantly (Que *et al.* 2020; Liu *et al.* 2022). Although the increase in ductility was not significant, the strength and stiffness of the joints in glued laminated timber with inclined STSs were greater than the joints with vertical STSs (Brown *et al.* 2021).

However, most of the relevant studies focused on comparing the mechanical performances of joints reinforced by STS and ordinary joints, while the arrangement of the STS and the influence of the insertion angle on the mechanical performance of the reinforced joints were less studied.

This study aimed to maximize the strength and stiffness of the moment-resisting joints reinforced by STS through deciding the optimal arrangement and insertion angle of STS. Four types of glulam joints reinforced by STS with different arrangements and insertion angles were prepared as the specimens, and the monotonic loading test and low-cycle reciprocating loading test were conducted to investigate the influence of the arrangement and the insertion angle on the mechanical properties of glulam joints. The failure modes, bearing performances, and energy dissipation capacities of the joints were discussed, and the optimal arrangement and insertion angle of STS to enhance the stiffness and ductility of glulam joints were determined. Furthermore, the flexural mechanical properties of the joints determined in this study provide a reference for using STS to connect glulam moment-resisting joints in engineering applications.

EXPERIMENTAL

Materials

To explore the influence of inclined screws and their geometric arrangement on the mechanical properties of moment-resisting timber joints, four types of specimens were designed: a moment-resisting joint with a circular arrangement and a 90° drilling angle (MC90), a moment-resisting joint with a circular arrangement and a 45° drilling angle (MC45), a moment-resisting joint with a rectangular arrangement and a 90° drilling angle (MR90), and a moment-resisting joint with a rectangular arrangement and a 45° drilling angle (MR45). Three specimens of each type were prepared for a total of 12 tests.

The radius formed by circularly arranging the screws was 90 mm and the square side length formed by the rectangular arrangement was 180 mm, which met the requirements of Eurocode 5: Design of timber structures (2008) for screw spacing, edge

spacing, and end spacing. Additionally, the screw placements were the same whether the screws were screwed into the wood vertically or obliquely, and whether in a circular or a square arrangement. Figure 1 provides dimension diagrams for the designed glulam moment-resisting joints.

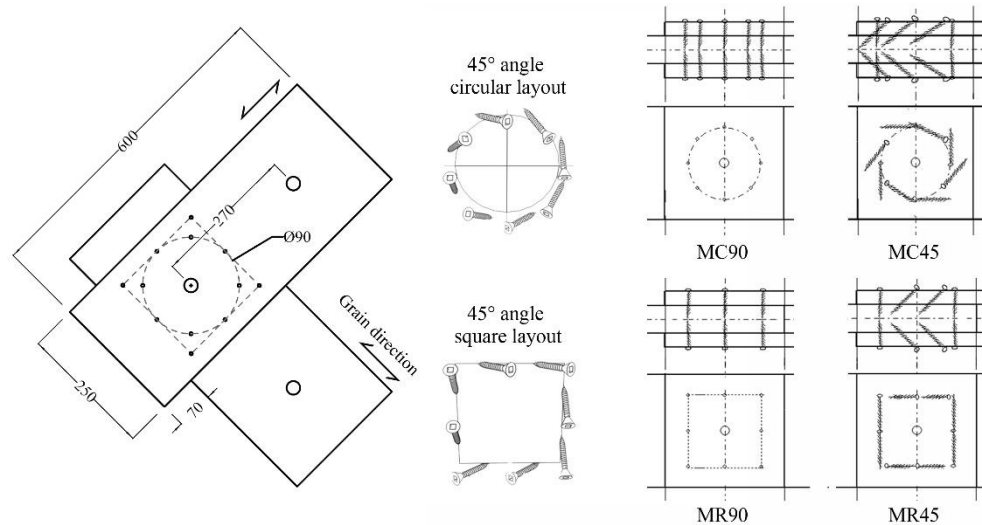


Fig. 1. Schematic diagram for the design and dimensions (in mm) of the moment-resisting joints

Each screw had to be driven along the normal plane of its assigned position and rotation center at an angle of 45° . The glulam was made of SZ1 American Douglas fir by cold pressing with single-component polyurethane and was produced by the factory at Jiangsu Huiyoulin Integrated Construction Technology Co., Ltd. It was pressurized for 4 hours at 1.0 MPa at room temperature of 25°C . The glue placement was controlled to 250 g/m^2 . After pressing, sawing, and sanding, the glulam specimens were 1,200 mm long and 250 mm wide, the auxiliary material was 50 mm thick, and the primary material was 100 mm thick.

According to ISO 13061-1 (2014) and ISO 13061-2 (2014), the moisture content of the glulam was 10.3% and the density was 510 kg/m^3 .

The screws used in the tests were American solid fully threaded STS with diameters of 6 mm and total lengths of 140 mm. The specific dimensions are shown in Fig. 2 and Table 1.

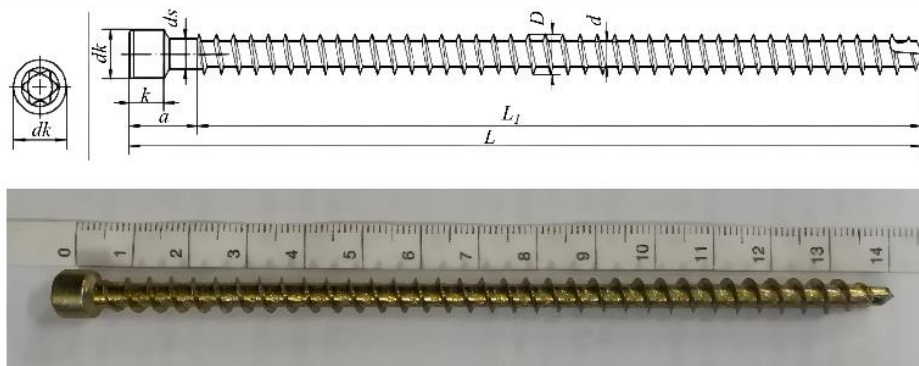


Fig. 2. Self-tapping screw for the experiment

Table 1. Dimensions of the Self-tapping Screw

Index	Screw Length L (mm)	Thread Length L_1 (mm)	Thread Diameter D (mm)	Rod Diameter d (mm)	Head Diameter d_k (mm)	Head Length K (mm)
Dimension	140.0	130.0	6.0	4.0	8.4	5.5

The bending yield strength and bending moment of the STS were tested according to EN 1380 (2009) and ASTM F1575 (2017), and the pull-out performance was tested according to EN 1382 (2016). The test results are shown in Table 2. The mean value and standard deviations are presented in the Table.

Table 2. Mechanical Properties of the Self-Tapping Screw

Index	Plastic Section Modulus S (mm ³)	Ultimate Yield Load P (N)	Moment M_y (N·mm)	Bending Strength F_y (MPa)	Pullout Strength F_b (MPa)
Mean value	11(±0.15)*	999(±224.29)*	11,558(±2,614.07)*	1,064(±235.69)*	25.79(±3.85)*

*The values in parentheses are standard deviations.

Methods

The cyclic loading tests used to explore the mechanical performance of this new type of glulam bending joint refer to ISO 16670 (2003). In this test, a 100kN universal mechanical testing machine (UTM5105, SANZI, China) was used for loading. Displacement control loading was used throughout the test, for which a downward compressive load was positive and an upward pulling load was negative. In the loading system, the target displacement value for each cyclic level was determined by the rotation angle of the joint, and the load was cycled three times for each level. The loading system is described in Table 3.

Table 3. Loading System for the Moment-resisting Joints

Cyclic Level	Number of Cycles	Rotation Angle (Rad)	Speed (mm/min)	Target (mm)
1	3	1/300	±2	±0.87
2	3	1/150	±2	±1.73
3	3	1/100	±2	±2.6
4	3	1/75	±4	±3.47
5	3	1/50	±6	±5.2
6	3	1/40	±8	±6.5
7	3	1/30	±10	±8.67
8	3	1/15	±12	±13
9	3	1/10	±12	±17.3
10	3	No limit	±12	until failure

In addition, four displacement meters with strokes of 50 mm were installed on the sides of the test specimens, and the distance between the displacement meters was 190 mm. The displacement meters were used to record the relative displacements of the main members and the side members of the joints during the tests, then the angles of the moment-resisting joints could be calculated. Because the main members consisted of two wood members, to ensure that the rotational deformation of the two wood members was

consistent, specific metal fixtures were used to connect the two wood members. Therefore, the main members could be regarded as a whole and the rotational deformation could be acquired by two displacement meters installed on the one side of the main members. The installation positions of the displacement meters are shown in Fig. 3(a), and the specific fixture after installation is shown in Fig. 3(b). The specific method of calculating the rotation angle, (α), is shown in Eq. 1.

$$\alpha = \frac{G_1(U_1 - U_2) + G_2(U_3 - U_4)}{2} \quad (1)$$

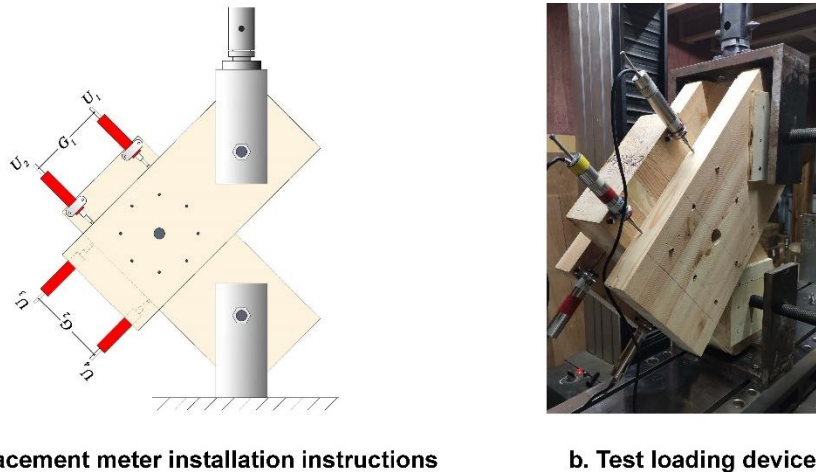


Fig. 3. Installation of the displacement meters and the test loading device

RESULTS AND DISCUSSION

Observed Damage

Figure 4 shows typical failure modes for the four types of specimens. The dominant failure mode of specimens with different STS configurations was all tearing failure along the centerline of the wood parallel to the grain.

The yield load of glulam joint was reached when the angular displacement was near $1/30$ rad during a test. In this stage, there were cracks in the wood near the screw located on the center line of the main and side materials, and wood-splitting phenomenon became more frequent. With increases in the cyclic load, the cracks began to propagate slowly.

The ultimate load of specimens was reached when the cyclic level reached the ninth or tenth level. Although there were tearing sounds of wood, the specimens did not fail immediately. However, when the cyclic load-displacement increased and the next cyclic load was applied, the maximum load of the previous cycle could not be reached and a split occurred instantly. After that, the load value decreased continuously until the test was terminated. The cracks propagating from the midpoint of the joint to the other side of the main member and side member were serious. Furthermore, the STSs at the connection zone of the glulam joints were bent due to the shear loading and embedded inside the wood instead of suffering fatigue failure, indicating that the glulam joints did not fail during earlier conditions of repeat cycles.

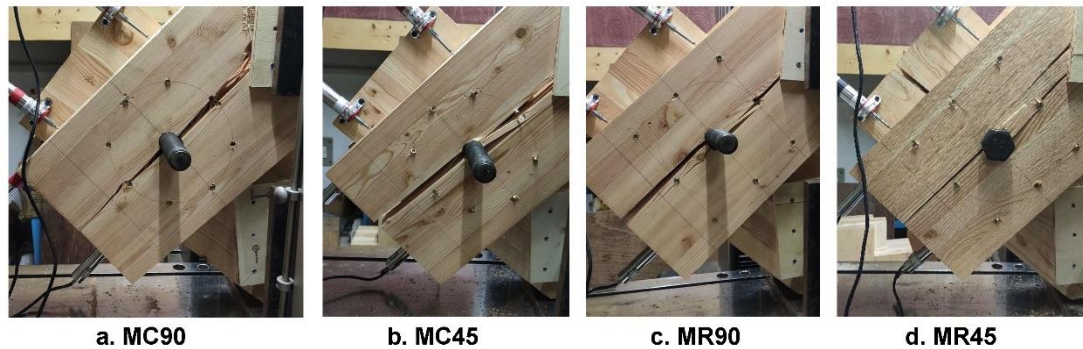


Fig. 4. Typical failure modes for each type of specimens

Hysteretic and Skeleton Curves

The data recorded by the four displacement meters installed on the test specimens were transformed into the relative rotation angles of the main members and side members of the test joints during the test process. At the same time, the load values of the mechanical test machine were transformed into the bending moments of the joints. The specific transformation method is shown in Fig. 5.

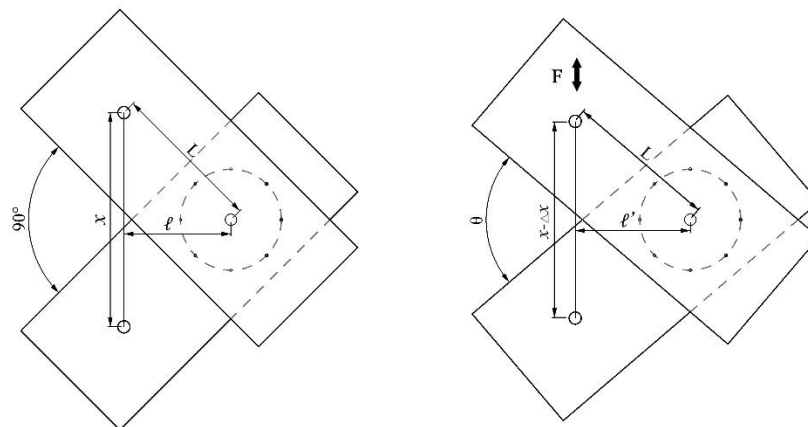


Fig. 5. Method of calculating the bending moment (dimensions in mm)

If the angle after rotation is θ , then Eqs. 2 and 3 apply:

$$\theta = 2\arcsin \frac{x-\Delta x}{2L} \quad (2)$$

$$\Delta\theta = 90^\circ - 2\arcsin \frac{x-\Delta x}{2L} \quad (3)$$

Then the moment, M_θ , corresponding to the rotation angle, $\Delta\theta$, could be obtained, as shown in Eq. 4,

$$M_\theta = F \cdot \ell' = F \cdot \sqrt{L^2 - \left(\frac{x-\Delta x}{2}\right)^2} \quad (4)$$

The final moment-rotation ($M-\theta$) curves for the tests could then be obtained by calculation. Figure 6 shows the moment-rotation curves for the third group specimens of each type. The relatively symmetrical hysteretic curves of timber joints with vertical screws indicate that the residual displacement of joints was relatively small under the repeat

cycles, which was consistent with the failure mode of joints. The specimens with the same insertion angle had very similar hysteresis curve trends. Specifically, the hysteresis curves for the 90° vertical specimens had center symmetry and typical reverse S-shapes, and the energy dissipation capacities for both the forward and reverse directions were essentially the same. However, the forward energy dissipation capacities for the 45° oblique specimens were significantly higher than in the reverse direction. This occurred primarily because each screw was inclined from the normal direction of the driving point and the rotation center, so all the screws were subjected to compressive loads. A node load could be uniformly supported in a tension–shear composite force state, thus significantly improving the forward energy dissipation capacity of the node. Additionally, in the compressive state, the 45° obliquely driven specimens had higher energy dissipation capacities than the 90° vertically driven specimens, while the opposite was true in the tensile state. The difference in the loading capacities and energy dissipation capacities of the specimens under compression and tensile state indicates that the moment-resisting joints connected only with inclined STSs are not suitable for the application in the tensile state.

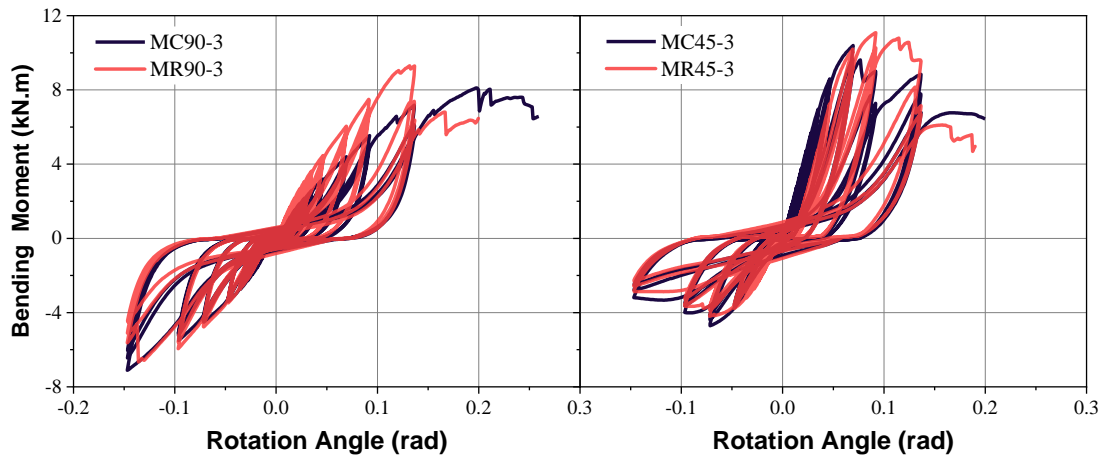


Fig. 6. Hysteretic curves for the moment-resisting timber joints

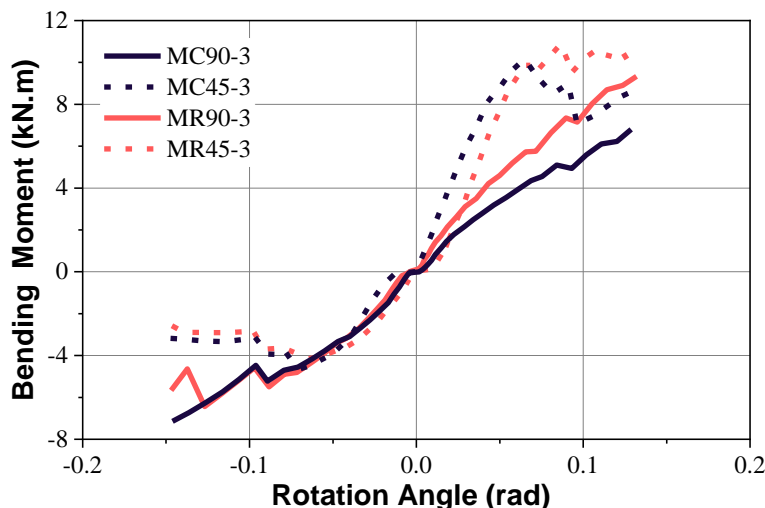


Fig. 7. Moment– θ envelope curves for the moment-resisting joints

A skeleton curve for each test specimen was obtained by connecting the envelope line around the first circle of each cyclic load level from the hysteretic curves. The initial rigidity, ductility, and other mechanical indexes for each group of test specimens could be calculated from the envelope line. The envelope lines for the four groups of test specimens are shown in Fig. 7.

The skeleton curves for the four groups of test specimens were analyzed. Each had an obvious initial elastic stage. However, when a specimen reached its maximum bending moment, the 90° vertically driven specimens (MC90 and MR90) showed more brittle failure. That is to say, when the maximum bending moments were reached, the ability of the joints to bear the bending moments dropped to less than 80% in an instant, accompanied by loud tearing sounds indicating the destruction of the short timber joints. However, when the 45° obliquely driven specimens (MC45 and MR45) reached their maximum bending moments under cyclic loading, the maximum bending moments also dropped sharply. The joints were not completely damaged and the bending moments could remain above 80% of the maximum bending moments, gradually climbing with subsequent increases in the cyclic displacement loads. Through the experiments, it was found that compared with MR45, MC45 was more prone to sudden load drops at the maximum bending moment. Therefore, MR45 had the best ductility and bending resistance of the four test specimens. The improvement of ductility and bending resistance of specimens with a rectangular arrangement could be attributed to the longer distance between the screw and the center of rotation compared to the specimens with a circular arrangement, which provided greater anti-rotational moments.

Analysis of the Joint Properties

Based on the analysis of the data in the positive and negative directions of each skeleton curve, the foundational mechanical properties of the 12 specimens, such as the initial rigidity and ductility were calculated. The results are shown in Table 4.

Table 4. Mechanical Properties for the Four Groups of Moment–Resisting Joints

Specimen	Moment (kN.m)		Stiffness (N.m/rad)		Ductility	
	Positive	Negative	Positive	Negative	Positive	Negative
MR90-1	7.77	5.78	75880.00	70186.30	1.66	2.44
MR90-2	9.39	8.58	84141.30	75758.00	1.50	1.59
MR90-3	9.30	6.67	92338.20	69233.20	1.53	1.84
AVG	8.82	7.01	84119.83	71725.83	1.56	1.96
MR45-1	7.75	7.78	135901.00	130308.00	2.55	1.71
MR45-2	11.20	4.24	170691.00	87199.30	2.15	2.17
MR45-3	11.09	4.20	150097.00	98603.70	2.08	2.55
AVG	10.01	5.41	152229.67	105370.33	2.26	2.14
MC90-1	7.44	3.74	33327.30	52751.30	1.40	1.58
MC90-2	7.24	5.61	65100.90	52040.20	1.48	1.75
MC90-3	7.18	7.11	66391.40	68507.20	1.49	1.77
AVG	7.29	5.49	54939.87	57766.23	1.46	1.7
MC45-1	5.80	4.82	71855.80	98354.50	2.06	2.06
MC45-2	12.59	4.05	207831.00	42514.40	1.74	1.54
MC45-3	10.40	4.71	200625.00	74432.30	3.17	1.90
AVG	9.60	4.53	160103.93	71767.07	2.32	1.83

In the compressed state, the inclined screw specimens (MC45 and MR45) had large anti-rotation bending moments, which were increased by 31.7% and 13.5%, respectively, compared with the vertical screw specimens (MC90 and MR90) under the same geometric arrangement. This occurred primarily because when it was considered in the experimental design stage that the nodes would bear downward compressive loads, the bending moments of the nodes would be uniformly dispersed in the form of shear forces according to the positions of the screws. Therefore, each screw was inclined from the normal direction of its driving point and rotation center so that all the screws would bear the compressive joint load evenly in the tension-shear composite force state, thereby significantly improving the anti-rotation bending moment of the node. However, in the tensile state, the oblique screw specimens were subjected to combined compression-shear forces, which led to the bending deformation of the tapping screw and significantly reduced the strength of the screw joints (Komatsu *et al.* 2019). Thus, the strengths of the screw joints were decreased by 17.5% and 22.9% respectively compared with the vertical screw specimens (MC90 and MR90) under the same geometric arrangement.

Judging from the data results for the two stress states, no matter which arrangement method was used, the method of driving the screws at an angle of 45° significantly improved the rotational stiffness and ductility of the joints. This occurred because the 90° vertical screw joints were primarily shear-resistant when resisting external forces. However, the 45° oblique screw joints were in tension-shear or compression-shear composite stress states when resisting external forces, and in addition to a shearing force, an anti-pulling force or an anti-extrusion force was generated with the base material. Thus, the mechanical properties of the bending joint were improved.

Stiffness Degradation and Energy Dissipation Capacity Comparisons

The test results for the four groups of specimens were further analyzed to obtain the secant stiffness and equivalent viscous damping coefficient for each cyclic loading stage for each test specimen. The results are shown in Figs. 9 and 10.

Another important index for measuring the performance of a joint under low-cycle repeated loading is the stiffness degradation coefficient (η_K), which can evaluate the stiffness degradation degree of the specimen after the i th cyclic loading state. The secant stiffness (K_i) was used as the effective stiffness for the i th cyclic loading stage, and it is defined by Eq. 5,

$$K_i = \frac{|+P_i|+|-P_i|}{|+\Delta_i|+|-\Delta_i|} \quad (5)$$

The stiffness degradation coefficient could then be calculated using Eq. 6,

$$\eta_K = \frac{K_i}{K_1} \quad (6)$$

where $+P_i$ and $-P_i$ represent the maximum load values in the forward and reverse directions in the i th cycle, respectively, $+\Delta_i$ and $-\Delta_i$ are the horizontal displacement values corresponding to the maximum load value of the i th cycle in the forward and reverse directions, respectively, and K_1 is the secant stiffness of the first cyclic load applied to the specimen.

Figure 8 shows that there was no stiffness degradation phenomenon during the early loading periods of the joints, but rather there were stiffness trends of first increasing and then decreasing. The stiffnesses of the MR90 and MC90 joints had similar trends: both increased step-by-step with increases in the number of load cycles during the early stage.

When the number of load cycles reached 15, that is, when the load–displacement reached 1/50 rad, the secant stiffness for a single cyclic load reached its peak. After that, it began to decline gradually, showing a stiffness degradation trend. This trend occurred because of the small displacement of the loading point during the initial cyclic loading stage. The tearing degree of the wood fibers entangled in the joint reduced when the arrangement of the STS in the bending joint was closer. Therefore, the bending stiffness of STS played a leading role. With increases in the load, the STS and the wood fibers were gradually pulled apart. With the combination of embedment pressure, screw shear, screw pull-out, and other composite forces, the joint stiffness began to increase gradually. Then the wood fibers wrapped around the STS pulled off gradually, the screws produced bending plastic hinges, the notches in the screws gradually increased, and the pin groove of the wood was compressed and crushed. At this point, the joint stiffnesses began to decline gradually until the joints were damaged. MC45 and MR45 showed nearly the same trend. From the initial loading stage, the joint stiffnesses gradually increased to the load–displacement of 1/50 rad, then showed a relatively stable trend until 1/10 rad was reached. Combined with the failure phenomenon, this kind of stiffness decreased rapidly after it reached its maximum, which explains the reason for the brittle failure of the glulam flexural joints connected by inclined screws after the specimens yielded. The analysis described above indicates that the influence of the screw insertion angle on the stiffness degradation of the specimens was significant, while the geometrical arrangement of the screws had no significant effect.

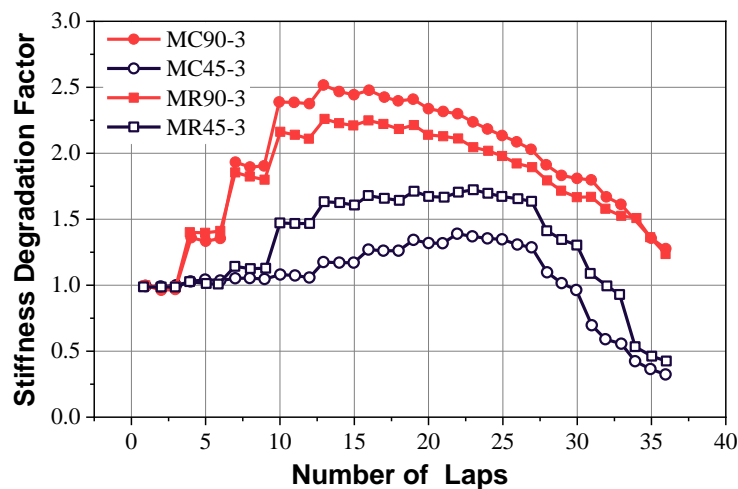


Fig. 8. Stiffness degradation for the four groups of moment-resisting timber joints

The hysteresis curves for the four groups of test specimens were relatively full, indicating that each had a certain energy dissipation capacity. The equivalent viscous damping coefficient (h_e) was generally used to characterize and compare the energy dissipation capacities of the four groups of test specimens. The equivalent viscous damping coefficient is essentially the ratio of the actual dissipated energy of a cyclic load to the theoretical dissipated energy of that cyclic load. A large equivalent viscous damping coefficient indicates a high energy dissipation capacity for the node.

Figure 9 shows that the energy dissipation capacity trends for the four groups of specimens were nearly the same. As the angular displacement increased, the energy dissipation capacities became increasingly stronger, especially for the 45° inclined screw specimens (MC45 and MR45), which had nearly the same trends. Before the 30th cyclic loading stage, the 90° vertical screw specimens had higher energy dissipation capacities,

while after that, the energy dissipation capacities of the 45° specimens increased significantly and exceeded those of the 90° specimens. This occurred primarily because the 45° specimens showed good ductility in the later loading stages, continuing to have a certain degree of structural deformation after reaching the maximum bearing capacity to consume part of the kinetic energy. Therefore, the energy dissipation capacities of the flexural joints were more affected by the screw-driving angle than by the geometric arrangement of the screws.

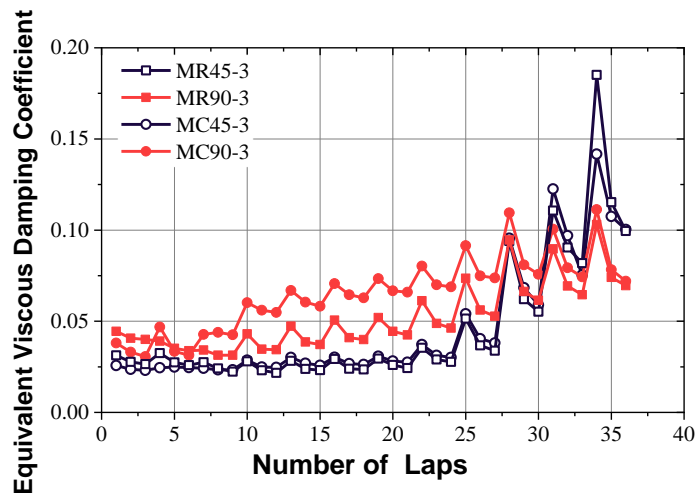


Fig. 9. Energy dissipation capacities for the four groups of moment-resisting timber joints

CONCLUSIONS

1. The specimens with the same screw-driving angles had very similar hysteretic curve trends. Under compression state, the 45° oblique screw specimens had higher anti-rotation bending moments than the 90° vertical screw specimens, which were increased by 31.7% (circular arrangement) and 13.5% (rectangular arrangement) under the same geometric arrangement. But under tensile state, the 45° oblique screw specimens were subjected to combined compression-shear forces, which led to the bending deformation of the tapping screw and significantly reduced the strength of the screw joints. The strength deductions were 17.5% (circular arrangement) and 22.9% (rectangular arrangement) under the same geometric arrangement.
2. The insertion angle of STS significantly affected the stiffness degradation and energy dissipation capacities of the wooden joint, while the geometric arrangement had no significant effect. In particular, the 45° oblique screw specimen with a square arrangement had the best ductility and stiffness.
3. Using self-tapping screws (STS) improved the mechanical properties of the wooden joint to a certain extent, but it had no outstanding advantage in the reverse tensile state. If STS are set in both the clockwise and counterclockwise directions of a joint, the forward and reverse flexural resistances of the joint may achieve a good balance. Furthermore, a combined approach of STS and glue to connected glulam joints simultaneously may further enhance the strength and stiffness of the joints, especially in the case of the reverse tensile state, and can be studied in future work.

ACKNOWLEDGMENTS

Shuo Wang and Panpan Ma contributed equally to this work. The authors are grateful for the support of the National Natural Science Foundation of China, Grant No. 31670566; the Research Project of Jiangxi Forestry Bureau, Grant No. 202013 and the Postgraduate Research & Practice Innovation Program of Jiangsu Province, Grant No. KYCX22-1080. In this study, glulam was provided by Jiangsu Huiyoulin Building Technology Co., Ltd. The fully threaded screws were provided by Shanghai Moregood Hardware Co., Ltd. The authors would like to express their sincere thanks for this support.

REFERENCES CITED

- ASTM F1575 (2017). "Standard test method for determining bending yield moment of nails," ASTM International, West Conshohocken, PA.
- Bejtka, I., and Bl, H. J. (2004). "Reinforcements perpendicular to the grain using self-tapping screws," in: *World Conference on Timber Engineering*, Lahti, Finland, pp. 233-239.
- Blaß, H. J., and Schadle, P. (2011). "Ductility aspects of reinforced and non-reinforced timber joints," *Engineering Structure* 33(11), 3018-3026. DOI: 10.1016/j.engstruct.2011.02.001
- Brown, J. R., Li, M.-H., Tannert, T., and Moroder, A. (2021). "Experimental study on orthogonal joints in cross-laminated timber with self-tapping screws installed with mixed angles," *Engineering Structures* 228. DOI: 10.1016/j.engstruct.2020.111560.
- EN 1380 (2009). "Timber structures - Test methods - Load bearing nails, screws, dowels and bolts," European Committee for Standardization, Brussels, Belgium.
- EN 1382 (2016). "Timber Structures - Test methods - Withdrawal capacity of timber fasteners," European Committee for Standardization, Brussels, Belgium.
- EN 1995-1-1 (2008). "Design of Timber Structures - Part 1-1: General-Common Rules and Rules for Buildings," European Committee for Standardization, Brussels, Belgium.
- Gehloff, M., Cloßen, M., and Lam, F. (2010). "Reduced edge distances in bolted timber moment connections with perpendicular to grain reinforcements," in: *World Conference on Timber Engineering*, Trentino, Italy, pp. 970-978.
- ISO 13061-1 (2014). "Physical and mechanical properties of wood. Test methods for small clear wood specimens. Part 1: Determination of moisture content for physical and mechanical tests," International Organization for Standardization, Geneva, Switzerland.
- ISO 13061-2 (2014). "Physical and mechanical properties of wood. Test methods for small clear wood specimens. Part 2: Determination of density for physical and mechanical tests," International Organization for Standardization, Geneva, Switzerland.
- ISO 16670 (2003). "Timber structure-Joints made with mechanical fasteners-Quasi-static reversed-Cyclic test method," International Organization for Standardization, Geneva, Switzerland.
- Jensen, J. L. (2005). "Quasi-non-linear fracture mechanics analysis of splitting failure in moment-resisting dowel joints," *Journal of Wood Science* 51(6), 583-588.

- Kasal, B., Heiduschke, A., Kadla, J., and Haller, P. (2004). "Laminated timber frames with composite fibre-reinforced connections," *Progress in Structural Engineering and Materials* 6(2), 84-93; DOI: 10.1002/pse.173
- Komatsu, K., Teng, Q., Li, Z., Zhang, X., and Que, Z. (2019). "Experimental and analytical investigation on the nonlinear behaviors of glulam moment-resisting joints composed of inclined self-tapping screws with steel side plates," *Advances in Structural Engineering* 22(15), 3190-3206. DOI: 10.1177/1369433219858722
- Lam, F., Closen, M., and Gehloff, M. (2010). "Moment-resisting bolted timber connections," *Structures & Building* 163(4), 267-274. DOI: 10.1680/stbu.2010.163.4.267
- Lam, F., Wrede, M., Yao, C., and Gu, J. (2008). "Moment resistance of bolted timber connections with perpendicular to grain reinforcements," in: *World Conference on Timber Engineering*, Miyazaki, Japan, pp.978-986.
- Liu, Y., Yao, Z., Wang, F., Huang, H., and Que, Z. (2022). "Utilization of wood-derived biomass as a liquid fuel source: Part 2," *J. Biotechnol. Bioenergy* 12(2), 153-162. DOI: 10.1016/0144-4565(90)90070-Z
- Mirdad, M. A. H., Jucutan, A., Khan, R., Niederwestberg, J., and Chui Y. (2022). "Embedment and withdrawal stiffness predictions of self-tapping screws in timber," *Construction and Building Materials*. DOI: 10.1016/j.conbuildmat.2022.128394
- Que, Z., Han, C., Teng, Q., Hu, C., and Luo, W. (2020). "Study on anti-side performance of glulam beam-column joints with inclined screw," *China Forest Products Industry* 57(05), 34-40. DOI: 10.19531/j.issn1001-5299.202005008 (in Chinese)

Article submitted: December 10, 2023; Peer review completed: January 3, 2024; Revised version received January 4, 2024; Accepted: February 29, 2024; Published: March 6, 2024.

DOI: 10.15376/biores.19.2.2626-2638